

Pinalites: Optical properties and Quantum Magnetism of Heteroanionic $A_3MO_5X_2$ Compounds

Daigorou Hirai*,†

†Department of Applied Physics, Nagoya University, Nagoya 464-8603, Japan

ABSTRACT: Heteroanionic compounds, which contain two or more types of anions, have emerged as a promising class of materials with diverse properties and functionalities. In this paper, I review the experimental findings on $Ca_3ReO_5Cl_2$ and related compounds that exhibit remarkable pleochroism and novel quantum magnetism. I discuss how the heteroanionic coordination affects the optical and magnetic properties by modulating the d-orbital states of the transition metal ions and then compare these materials with other heteroanionic and monoanionic compounds and highlight the potential of $A_3MO_5X_2$ materials for future exploration of materials and phenomena.

1. INTRODUCTION

Heteroanionic compounds, which contain two or more types of anions, have unique crystal structures and properties that are not found in monoanionic compounds such as oxides¹. Heteroanionic compounds have been explored less than monoanionic compounds, but recent research has revealed various physical and chemical phenomena, such as superconductivity in $LaOFePn$ ($Pn = P, As$)^{2,3}, Li_xHfNCl_4 and $(Ca_{1-x}Na_x)CuO_2Cl_2$ ⁵, high dielectric constants in AMo_2N ($A = Ba, Sr, Ca$; $M = Ta, Nb$)⁶, ion conductivity in $LaOCl$ ⁷ and La_2LiHO_3 ⁸, catalytic activity in $BaTiO_{3-x}H_x$ ⁹ and $TaON$ ¹⁰, and the thermoelectric properties of $MCuOCh$ ($M = Bi, La$; $Ch = S, Se, Te$)^{11,12}.

One of the heteroanionic compounds that has attracted much attention is the oxychloride $Ca_3ReO_5Cl_2$ (known as CROC), which exhibits a remarkable optical property called pleochroism; that is, the color changes depending on the viewing direction and the polarization of the incident light. While pleochroism is an optical property found in a wide variety of minerals, CROC shows a dramatic change in color, from green to yellow to red, depending on the direction of polarization. CROC also shows novel quantum magnetism as a result of magnetic frustration. These properties are related to the heteroanionic coordination of the transition metal ion, which is influenced by the presence of both oxygen and chlorine anions. Several other compounds with similar characteristics have been synthesized and investigated, and they have the general formula $A_3MO_5X_2$.

In this review, I summarize the crystal structural features and the recent studies on the optical and magnetic properties of $A_3MO_5X_2$ compounds, with a focus on the role of the heteroanionic coordination. I also compare these compounds with other heteroanionic and monoanionic compounds and discuss the future prospects of Pinalite family ($A_3MO_5X_2$ materials). In the field of optical properties and quantum magnetism, where systematic material exploitation of heteroanionic compounds has been less developed, Pinalite compounds are a good model case for the usefulness of heteroanionic nature.

1.1 Pinalites: $A_3MO_5X_2$ COMPOUNDS

$A_3MO_5X_2$ compounds are a series of heteroanionic compounds with different combinations of A, M, and X ions. One of this group of compounds, $Pb_3WO_5Cl_2$, was first found in the mineral pinalite in Arizona^{14,15}, and, here, the $A_3MO_5X_2$ compounds are named “Pinalites”. Table 1 lists the reported compounds so far. In these materials, alkaline earth metals and Pb occupy the A site as A^{2+} ions, early transition metals (Mo, Re, and W) occupy the M site as M^{6+} ions, and halogens Cl and Br occupy the X site as X^- ions.

Since the discovery of CROC, compounds with Re^{6+} ions in the $5d^1$ electron configuration at the M site have been studied extensively, and their optical and magnetic properties have been of great interest. $A_3MO_5X_2$ compounds have two different types of crystal structures, as shown in Fig. 1a: the $Ca_3WO_5Cl_2$ -type structure in the $Pnma$ space group having $A = Ca$, and a $Pb_3WO_5Cl_2$ -type structure in the $Cmcm$ space group (or $Amam$, which has the same symmetry but different axis settings) for other compounds. The difference between the two structures is the distortion caused by the smaller ionic size of Ca^{2+} compared to other A^{2+} ions¹³.

1.2 $Pb_3WO_5Cl_2$ -TYPE STRUCTURE

Most compounds in the $A_3MO_5X_2$ family crystallize in the $Pb_3WO_5Cl_2$ -type structure. The $Pb_3WO_5Cl_2$ -type structure can be viewed as a layered structure with alternating layers of A_3MO_5 and X_2 . The A_3MO_5 layer is derived from the $[Pb_2O_2]$ layer in the structure of the mineral litharge, α - PbO ¹⁶, which is a common motif in lead halides¹⁷. The $[Pb_2O_2]$ layer consists of a square lattice of oxide atoms and a checkerboard arrangement of Pb atoms above and below the center of the oxygen squares. The A_3MO_5 layer also has a square lattice of oxide atoms at the O1 sites, but this lattice is corrugated. As shown in Fig. 1b, three-fourths of the Pb atoms in the $[Pb_2O_2]$ layer are replaced by A atoms in the A_3MO_5 layer, and the remaining one-fourth are replaced by

M-O units. The corrugations of the oxygen square lattice in the A_3MO_5 layer are due to the different sizes and shapes of the M-O units and the A cations.

The X_2 layers between the A_3MO_5 layers also form a square lattice that matches the opposite side of the protruding A

ion and the M-O unit. There are two X sites: X1 facing the A ion and X2 facing the M-O unit. The distance between X2 and the M-O unit is slightly shorter than that between X1 and the A ion, resulting in a slight distortion of the X square lattice.

Table 1. Compounds with the general chemical formula $A_3MO_5X_2$. The space group for $Pb_3WO_5Cl_2$ -type structure is standardized to *Cmcm*. ATL stands for anisotropic triangular lattice.

Chemical formula	Space group	Electronic configuration	Lattice constants (Å)	Unit cell volume (Å ³)	Comments	Ref.
$Ca_3ReO_5Cl_2$	<i>Pnma</i> (#62)	5d ¹	$a = 11.8997(2)$ $b = 5.5661(1)$ $c = 11.1212(2)$	$V = 736.61(2)$	Pleochroism ATL magnet ($J'/J = 0.25$) $T_N = 1.13$ K	18,19
$Ca_3ReO_5Br_2$	<i>Pnma</i> (#62)	5d ¹	$a = 12.1219(14)$ $b = 5.6447(7)$ $c = 11.2205(10)$	$V = 767.76(15)$	ATL magnet ($J'/J = 0.25$) $T_N = 1.15$ K	20
$Ca_3WO_5Cl_2$	<i>Pnma</i> (#62)	5d ⁰	$a = 11.820(2)$ $b = 5.587(1)$ $c = 11.132(1)$	$V = 735.2$	Charge transfer luminescence	21,22
$Sr_3ReO_5Cl_2$	<i>Cmcm</i> (#63)	5d ¹	$a = 5.6492(3)$ $b = 13.1886(6)$ $c = 11.1144(5)$	$V = 828.09(7)$	ATL magnet ($J'/J = 0.35$) $T_N < 1.8$ K	23
$Sr_3ReO_5Br_2$	<i>Cmcm</i> (#63)	5d ¹	$a = 5.7145(3)$ $b = 13.3445(7)$ $c = 11.3044(6)$	$V = 862.05(8)$	ATL magnet ($J'/J = 0.25$) $T_N < 1.8$ K	20
$Ba_3ReO_5Cl_2$	<i>Cmcm</i> (#63)	5d ¹	$a = 5.79424(18)$ $b = 13.9508(4)$ $c = 11.4414(5)$	$V = 924.86(5)$	ATL magnet ($J'/J = 0.40$) $T_N < 1.8$ K	23
$Ba_3ReO_5Br_2$	<i>Cmcm</i> (#63)	5d ¹	$a = 5.87477(4)$ $b = 14.1992(2)$ $c = 11.60519(9)$	$V = 968.07(4)$	ATL magnet ($J'/J = 0.45$) $T_N < 1.8$ K	20
$Ba_3WO_5Cl_2$	<i>Cmcm</i> (#63)	5d ⁰	$a = 5.796(2)$ $b = 13.825(2)$ $c = 11.469(2)$	$V = 919.01$		24
$Pb_3ReO_5Cl_2$	<i>Cmcm</i> (#63)	5d ¹	$a = 5.59462(4)$ $b = 13.26905(8)$ $c = 10.97535(7)$	$V = 814.33(3)$	ATL magnet ($J'/J = 0.35$) $T_N < 1.8$ K	20
$Pb_3WO_5Cl_2$	<i>Cmcm</i> (#63)	5d ⁰	$a = 5.617(1)$ $b = 13.067(3)$ $c = 11.073(2)$	$V = 812.81(3)$	Mineral: pinalite	14,15
$Pb_3WO_5Br_2$	<i>Cmcm</i> (#63)	5d ⁰	$a = 5.677(2)$ $b = 13.323(3)$ $c = 11.217(3)$	$V = 848.4$		16
$Pb_3MoO_5Cl_2$	<i>Cmcm</i> (#63)	4d ⁰	$a = 5.59485(5)$ $b = 13.1149(2)$ $c = 11.0116(1)$	$V = 807.98(1)$		16

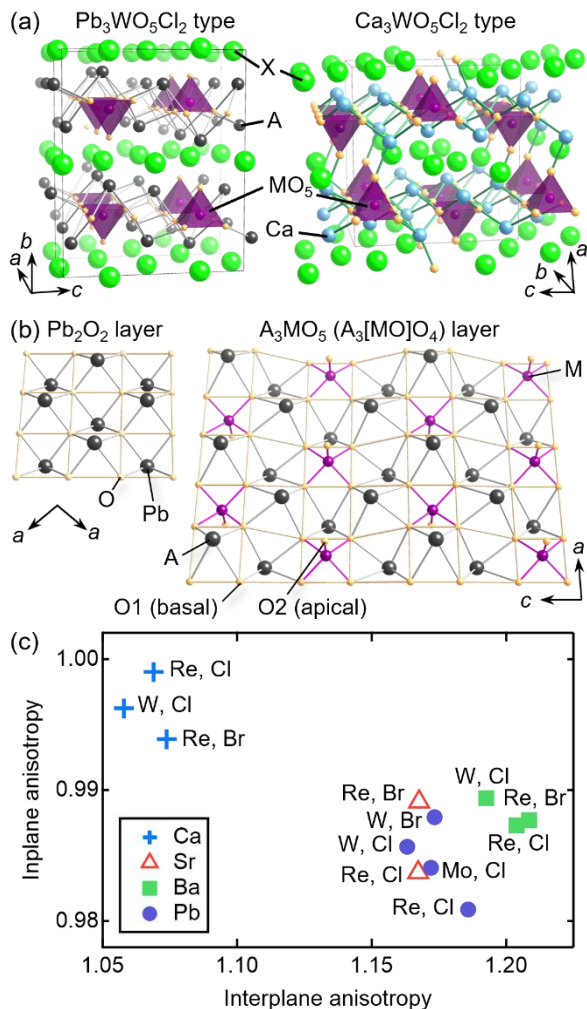


Figure 1. (a) Crystal structures of $\text{Pb}_3\text{WO}_5\text{Cl}_2$ -type in $Cmcm$ (left) and $\text{Ca}_3\text{WO}_5\text{Cl}_2$ -type in $Pnma$ (right). Both structures commonly contain the A_3MO_5 layer. (b) Comparison between the $[\text{Pb}_2\text{O}_2]$ layer in $\alpha\text{-PbO}$ (left) and the A_3MO_5 layer (right). Square lattice formed by oxide atoms are common in both layers, but the square lattice in the A_3MO_5 layer is corrugated. In the $[\text{Pb}_2\text{O}_2]$ layer, Pb atoms are located above and below the center of the oxygen squares in a checkerboard pattern. In the A_3MO_5 layer, A atoms and M-O units are arranged in a similar manner to that of Pb atoms in the $[\text{Pb}_2\text{O}_2]$ layer. (c) The inplane and interplane anisotropies of the A_3MO_5 layers in $\text{A}_3\text{MO}_5\text{X}_2$ compounds calculated from the lattice constants.

The M^{6+} ion is surrounded by four basal oxygen atoms (O1) and one apical oxygen atom (O2), forming an MO_5 square pyramidal coordination. The M-O2 bond distance is shorter than the M-O1 bond distance, and the M^{6+} ion is off the oxygen square plane. The unusual square pyramidal coordination of the M^{6+} ion is likely influenced by the X ion on the opposite side of the apical oxygen.

The A^{2+} ion has two sites: A1 and A2. A1 is coordinated by four basal oxide atoms (O1) and four X ions in a square antiprismatic geometry. A2 is also bonded to four basal oxide atoms and four X atoms, but in addition, it is bonded to the

apical oxygen (O2) of the neighboring A_3MO_5 layer, resulting in a nine-coordinated monocapped square antiprism.

1.3 $\text{Ca}_3\text{WO}_5\text{Cl}_2$ -TYPE STRUCTURE

When the A-site ion is Ca^{2+} , $\text{A}_3\text{MO}_5\text{X}_2$ compounds crystallize in the $\text{Ca}_3\text{WO}_5\text{Cl}_2$ -type structure (Fig. 1a). The $\text{Ca}_3\text{WO}_5\text{Cl}_2$ and $\text{Pb}_3\text{WO}_5\text{Cl}_2$ -type structures both have an A_3MO_5 layer, but they differ in the X layer. In the $\text{Pb}_3\text{WO}_5\text{Cl}_2$ -type structure, the X layer forms a square lattice, but in the $\text{Ca}_3\text{WO}_5\text{Cl}_2$ -type structure, the X layer is broken into one-dimensional (1D) slabs along the b axis. This is because the Ca ions are too small to form a $\text{Pb}_3\text{WO}_5\text{Cl}_2$ -type structure, and the coordination numbers of the Ca^{2+} ions are reduced to five or six, compared to eight or nine for other A^{2+} ions. Further, one of the three Ca^{2+} ion in the $\text{Ca}_3\text{WO}_5\text{Cl}_2$ -type structure is strongly bonded to the apical oxygen of the M-O unit in the adjacent A_3MO_5 layer, in addition to the four basal oxygens. This leaves no room for the X ions, and the X square lattice is, thus, split into slabs.

In the $\text{Ca}_3\text{WO}_5\text{Cl}_2$ -type structure, the M^{6+} ion also has a square pyramidal coordination, but the basal oxygen atoms form a trapezoid instead of a rectangle, as in the $\text{Pb}_3\text{WO}_5\text{Cl}_2$ -type structure. This symmetry change affects the electronic properties, such as the optical and magnetic properties.

1.4 COMPARISON BETWEEN COMPOUNDS

Table 1 shows the lattice constants and unit cell volumes of $\text{A}_3\text{MO}_5\text{X}_2$ compounds. Changing the transition metal ion (M^{6+}) has little effect on the overall structure, and the volume change is less than 1%. This is reasonable because transition metal ions have similar ionic radii¹³. On the other hand, substituting the X^- and A^{2+} ions results in a significant structural change. To date, only materials with Cl^- and Br^- at the X site have been synthesized. Br^- , which has a larger ionic radius than Cl^- , increases the unit cell volume (V) by more than 4%. The A-site cation has the largest effect on the unit cell volume: comparing $\text{A}_3\text{ReO}_5\text{Cl}_2$ compounds, when $A = \text{Pb}$, Sr , and Ba , V is 10.6%, 12.4%, and 25.6% larger than that of $A = \text{Ca}$, respectively.

The inplane and interplane anisotropies of the A_3MO_5 layers, which are approximately $c/2a$ and $b/2a$, respectively, are compared in Fig. 1c (For $A = \text{Ca}$, the inplane and interplane anisotropies are $c/2b$ and $a/2b$). For $\alpha\text{-PbO}$ with a square lattice, the inplane anisotropy is one. All compounds are in the range $0.98 < c/2a < 1$, indicating that the square lattice formed by oxide atoms in the A_3MO_5 layer is close to a regular square lattice. The interplane distance is given by $a/2$ and $b/2$ for $\text{Ca}_3\text{WO}_5\text{Cl}_2$ - and $\text{Pb}_3\text{WO}_5\text{Cl}_2$ -type structures and varies from a minimum of 5.91 Å for $\text{Ca}_3\text{WO}_5\text{Cl}_2$ to 7.10 Å for $\text{Ba}_3\text{ReO}_5\text{Br}_2$. When normalized by the inplane lattice constants (b and a), compounds with a $\text{Ca}_3\text{WO}_5\text{Cl}_2$ -type structure have a smaller interplane anisotropy. This indicates that the $\text{Pb}_3\text{WO}_5\text{Cl}_2$ -type structure is more two-dimensional (2D) than the $\text{Ca}_3\text{WO}_5\text{Cl}_2$ -type structure.

For $M = \text{Re}$, $\text{A}_3\text{MO}_5\text{X}_2$ compounds with most combinations of $A = \text{Ca}$, Sr , Ba , and Pb and $X = \text{Cl}$ and Br have been synthesized. Because Re , Mo , and W ions have similar ionic radii

and electronegativities, compounds with $M = \text{Mo}$ and W can probably be synthesized on further investigation. $\text{Ba}_3\text{MoO}_5\text{Cl}_2$ has been synthesized, although not in a pure phase¹⁶. Despite the limited number of ions that can have the 6+ valence state, it may be possible to synthesize materials with Os^{6+} , Ru^{6+} , and Cr^{6+} at the M site in the future.

1.5 RELATED STRUCTURES

The $\text{Pb}_3\text{WO}_5\text{Cl}_2$ -type structure is related to that of lead molybdenum oxychloride: $\text{Pb}_7\text{MoO}_9\text{Cl}_2$ ¹⁶, known as the mineral parkinsonite²⁵. This composition can be expressed as $\text{Pb}_3\text{MoO}_5[\text{Pb}_4\text{O}_4]\text{Cl}_2$, which can be regarded as a stacked structure of A_3MO_5 , Pb_2O_2 , and X_2 layers. Unlike the $\text{Pb}_3\text{WO}_5\text{Cl}_2$ -type structure, in this structure, the Mo-O units randomly occupy the Pb sites²⁶. It has been reported that analogous compounds having a composition of $\text{Pb}_7\text{MO}_9\text{X}_2$ ($M = \text{Mo}, \text{W}$; $\text{X} = \text{Cl}, \text{Br}, \text{I}$)²⁷ can be synthesized. By adjusting the synthetic conditions and selecting the constituent elements, it may be possible to obtain $\text{A}_7\text{MO}_9\text{X}_2$ -type compounds with ideal stacking.

The $[\text{Pb}_2\text{O}_2]$ layer is structurally similar to the $[\text{Bi}_2\text{O}_2]$ layer in a series of materials with Aurivillius phases^{28,29}. As in the Aurivillius compounds with alternating octahedral $n\text{ABO}_3$ perovskite and $[\text{Bi}_2\text{O}_2]$ layers, the incorporation of perovskite octahedral layers between the A_3MO_5 layers is expected to further expand the structural diversity.

2 OPTICAL PROPERTIES

A remarkable physical property of CROC is its striking pleochroism (Fig. 2b). The color of crystals changes from green to reddish brown depending on the viewing direction (without polarizer), and the color changes from red to yellow to green depending on the polarization of the incident light (with polarizer). The heteroanionic coordination plays a crucial role in determining the optical properties.

2.1 VIOLATION OF LAPORTE RULE

$d-d$ transitions, in which electrons are excited between d -orbitals upon photoabsorption, are responsible for the color of many transition metal compounds. $d-d$ transitions also contribute to the pleochroism of CROC. In transition metal compounds, the energy levels of the five-fold degenerate d -orbitals of transition metal ions are split by the crystal field (so-called crystal field splitting (CFS)), as shown in Fig. 2a. The energy difference between the split d orbitals corresponds to the energy of visible light ranging from 1.5 to 3.5 eV. Therefore, by absorbing light with an energy matching the splitting, the electrons in the ground state d -orbital are excited, and the complementary color of the absorbed light becomes the color of the material. For example, in rubies, yellow-green light is absorbed by the $d-d$ transition of Cr^{3+} ions substituted for Al in Al_2O_3 , resulting in a complementary color: red³⁰⁻³².

However, $d-d$ transitions do not always occur. In particular, in the presence of an inversion center at the transition metal site, the $d-d$ transition is forbidden, and this is known as the Laporte selection rule³³. For monoanionic compounds, the

coordination is mostly tetrahedral or octahedral depending on the relative ionic sizes of the transition metal ions and anions. Many oxides have centrosymmetric octahedral coordination, in which there is an inversion center at the transition metal site. Thus, the $d-d$ transition is forbidden, and no light absorption occurs; thus, there is no color.

To violate the Laporte rule and achieve intense optical absorption, coordination without an inversion center at the transition metal site is necessary. A good example is the recently discovered vibrant blue pigment YInMn Blue, which consists of $\text{YIn}_{1-x}\text{Mn}_x\text{O}_3$ ³⁴. In this material, the transition metal ion responsible for optical absorption, Mn^{3+} , has a trigonal bipyramidal coordination without an inversion center at the transition metal site, which allows $d-d$ transitions. This unique coordination enables intense absorption of visible light, resulting in vibrant pigments. Other inorganic pigments with various colors have also been produced, mainly focusing on trigonal bipyramidal coordination³⁵.

Crucially, heteroanionic compounds have the advantage of violating the Laporte rule and achieving intense optical absorption. In heteroanionic coordination, multiple species of anions coordinate to the transition metal ion, making it easier to achieve low-symmetry noncentrosymmetric coordination. In particular, replacing one vertex of the MO_6 octahedron with one chloride ion, as shown in Fig. 2a, results in the loss of the inversion center at the transition metal site and, thus, allows $d-d$ transitions. In CROC, the Re^{6+} ion is surrounded by a square pyramidal coordination of five oxide atoms and one chlorine atom (Fig. 2a), which allows light absorption via the $d-d$ transition.

2.2 COMPLEX CFS

Heteroanionic coordination plays an important role not only in the intensity of light absorption but also in the energy of light absorption. In the case of octahedral coordination of oxides, CFS splits the d -orbital into a doubly degenerate e_g and a triply degenerate t_{2g} symmetry orbitals. Therefore, the only energy at which the transitions occur upon photoabsorption lies between e_g and t_{2g} levels (Fig. 2a).

In contrast, in CROC, the e_g and t_{2g} orbitals are further split by heteroanionic coordination: the divalent apical oxide atom in the z direction is replaced by a monovalent chloride ion with a longer interatomic distance, so that the d_{z^2} and $d_{x^2-y^2}$ orbitals in the e_g symmetry orbitals are significantly separated and the d_{yz}/d_{zx} and d_{xy} orbitals of t_{2g} symmetry are also split. Furthermore, the degenerate d_{yz}/d_{zx} orbitals split slightly into two linear combinations, d_{xz-yz} and d_{xz+yz} , as a result of the deformation of the basal square of oxide atoms to a trapezoid because of the chemical pressure from Ca^{2+} ions. The energies from the ground state d_{xy} orbital to the second highest d_{z^2} orbital and the highest $d_{x^2-y^2}$ orbital correspond to the energies of red and green light, respectively. These complex energy levels lead to the absorption of light at various wavelengths, resulting in the pleochroism of different colors depending on the viewing direction. This complex CFS has been observed in other heteroanionic compounds and are often discussed in relation to the spin states³⁶.

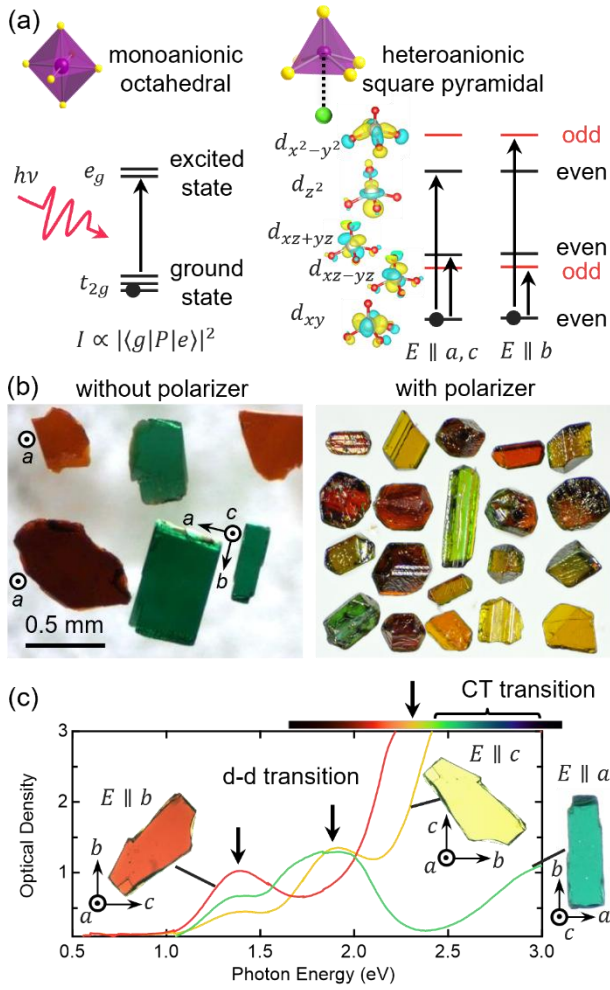


Figure 2. (a) Comparison of crystal field splitting of d-orbitals between monoanionic octahedral coordination (left) and heteroanionic square-pyramidal coordination of CROC (right). The parity of orbitals with respect to the mirror plane perpendicular to the b axis is shown on the right. (b) Photo of single crystals of CROC taken without (left) and with (right) polarizer. (c) Optical density spectra for CROC with linearly polarized incident light parallel to each axis. The corresponding photos of crystals are shown. The arrows indicate the absorption peaks corresponding to $d-d$ transitions. The intense absorption for $E \parallel b$ and c above 2.4 eV is attributed to the charge transfer transition.

2.3 MECHANISM OF PLEOCHROISM

As shown in Fig. 2c, CROC is trichroic, meaning that when the polarization of the incident light is parallel to the b , c , and a axes, the crystal colors are red, yellow, and green, respectively. The optical density spectra for the linearly polarized light of CROC show absorption peaks originating from $d-d$ transitions and broad and intense absorption originating from charge transfer (CT) transitions. As mentioned above, $d-d$ transitions are allowed in CROC because of the absence of local inversion symmetry at the transition metal site. CT transitions, which are generally Laporte-allowed

transitions between ligands and transition metal ions, exhibit intense optical absorption at higher energies than the $d-d$ transitions. In addition, $d-d$ transitions tend to have narrower absorption peaks because the bands of the d-orbitals are sharper than those of the p-orbitals of the ligand. Based on these characteristics, the absorption peaks at 1.4, 1.9, and 2.3 eV can be assigned as $d-d$ transitions, and continuous intense absorption above 2.4 eV for $E \parallel b$ and c and above 3.0 eV for $E \parallel a$ can be assigned as CT transitions. The pleochroism of CROC is attributed to the strong polarization dependence of the three $d-d$ and CT transitions.

First, the polarization dependence of the $d-d$ transition can be explained by considering the d-orbital arrangement split by the CFSs and the optical selection rule for electronic transitions. According to Fermi's golden rule, the probability of an electronic transition, i.e., the intensity of optical absorption, is proportional to the transition dipole moment, as follows:

$$I \propto |\langle g|P|e \rangle|^2$$

where e , g , and P denote the excited state, ground state, and the dipole moment of light, respectively. Electronic transitions are allowed when the transition dipole moment is finite. This is when the combination of the parities of the three components is even; in the CROC case, we consider the parities of the three components with respect to a mirror plane perpendicular to the b axis, which is the local symmetry of the Re site. The parity of each d orbital is shown in Fig. 2a, where the ground state d_{xy} orbital (g) is even, the excited states (e) d_{xz+yz} and d_{z^2} are even, and d_{xz-yz} and $d_{x^2-y^2}$ are odd. The parity of the light (P) is different depending on the polarization; light polarized along the b axis ($E \parallel b$) has odd parity with respect to the mirror plane, and light polarized along the a or c axis ($E \parallel a$ or c) has even parity.

Because the ground state (g) is a d_{xy} orbital with even parity, electronic transitions are allowed only when e and P have the same parity. In other words, when P is odd ($E \parallel b$) transitions to the d_{xz-yz} and $d_{x^2-y^2}$ orbitals where e is odd occur (Fig. 2a). On the other hand, when P is even ($E \parallel a$ or c), transitions to the d_{xz+yz} and d_{z^2} orbitals with even parity occur. The $d-d$ transitions at 1.4 and 2.3 eV observed for $E \parallel b$ correspond to excitations to the d_{xz-yz} and $d_{x^2-y^2}$ orbitals, while the transitions at 1.4 and 1.9 eV for $E \parallel a$ and c correspond to excitations to the d_{xz+yz} and d_{z^2} orbitals. The fact that the $d-d$ transitions to the d_{xz-yz} and d_{xz+yz} orbitals are observed at almost the same energy implies that the energy splitting between the two orbitals is small, as expected from the small trapezoidal distortion at the base of the ReO_5 square pyramid.

The difference in color between light polarized along the a and c axes comes from the energy difference in the CT transitions: in CROC, the ReO_5 square pyramids are aligned along the a axis, and light polarized along the a axis induces transitions from the p_z orbital of the apical oxygen to the Re d_{z^2} orbital. On the other hand, light polarized along the c axis induces transitions from p orbitals of the basal oxygen and the other Re 5d orbitals (d_{xy} , d_{xz-yz} , d_{xz+yz} , and $d_{x^2-y^2}$). It is possible that the strong hybridization of p_z and d_{z^2} is the origin

of the higher CT transition energies for $E \parallel a$ (above 3.0 eV) than those for $E \parallel c$ (above 2.4 eV). As described above, heteroanionic coordination, which violates Laporte rule and induces unique CFS, plays an important role in the pleochroism exhibited by CROC.

2.4 OUTLOOK AND OTHER OPTICAL PROPERTIES

The pleochroism of CROC is very sensitive to the coordination of the Re^{6+} ions. Therefore, the color can be controlled by replacing the ions at the A and X sites. In fact, our preliminary experiments have shown that replacing the A site with Sr and Ba increases the distance between Re^{6+} and the ligands and weakens the CFS, resulting in redshifted spectra. By growing single crystals of other $\text{A}_3\text{MO}_5\text{X}_2$ compounds, materials that exhibit pleochroism with different color variations from CROC can be synthesized. Therefore, violating the Laporte rule using heteroanionic coordination and enabling intense light absorption may be an effective strategy for developing new pigments. New pigments could be obtained by using a square pyramid and other heteroanionic coordination compounds.

Even in heteroanionic compounds without d-electrons, optical properties that are not observed in monoanionic compounds can be expected. For example, $\text{Ca}_3\text{WO}_5\text{Cl}_2$ with W^{6+} ions in the $5d^0$ electronic configuration has been investigated for its luminescence properties; notably, $\text{Ca}_3\text{WO}_5\text{Cl}_2$ exhibits blue luminescence under UV light illumination because of the CT transition between W^{6+} and the ligand ions²². Compared with the monoanionic compound Ca_3WO_6 , the luminescence band is redshifted by 0.36 eV. In contrast to monoanionic compounds, which have limited variation in the coordination polyhedra, heteroanionic compounds allow fine control of the CFS, which may also enable control of the luminescence properties. CT fluorescence of several heteroanionic tungsten compounds has already been reported^{37–39}: BaWO_2F_4 , which forms a distorted octahedron of $\text{cis}[\text{WO}_2\text{F}_4]^{2-}$, has shown green luminescence with high quantum yield³⁹. I hope that the luminescence properties of $\text{A}_3\text{MO}_5\text{X}_2$ compounds other than $\text{Ca}_3\text{WO}_5\text{Cl}_2$ will be investigated to discover desirable and highly efficient phosphors and scintillators.

In $\text{A}_3\text{MO}_5\text{X}_2$ compounds, the crystal structure has global inversion symmetry. However, heteroanionic coordination without a local inversion center sometimes leads to non-centrosymmetric crystal structures. Such structures cause nonlinear optical properties such as second-harmonic generation. Heteroanionic compounds have attracted increasing attention as new nonlinear optical materials^{40,41}. In the future, nonlinear optical properties will also be an important direction to explore in $\text{A}_3\text{MO}_5\text{X}_2$ compounds.

3 MAGNETIC PROPERTIES

The 5d electrons of the Re ions exhibit unique quantum magnetism. CFS arising from heteroanionic coordination gives rise to a spin state distinct from that of other 5d magnets and a low dimensionality derived from selective orbital occupation.

3.1 STABILIZATION OF THE SPIN-1/2 STATE

In many 3d transition-metal-based magnets, the orbital angular momentum is quenched; therefore, the spin quantum number S is a good quantum number without considering the spin-orbit interactions (SOIs). In contrast, 5d electrons usually have strong SOIs, forming an electronic state in which the spin and orbital angular momenta are entangled^{42–44}.

The electronic state of the 5d orbital is described by the spin-orbit-entangled $J_{\text{eff}} = 3/2$ states in compounds with octahedrally coordinated Re^{6+} ions in a $5d^1$ electronic configuration (Fig 3a). The effective orbital angular momentum $l_{\text{eff}} = 1$ derived from the triply degenerate t_{2g} orbitals coupled with the spin angular momentum $s = 1/2$ renders the total angular momentum $J_{\text{eff}} = 3/2$ a good quantum number. The cancellation between the spin momentum and effective orbital momentum results in the total magnetic moment M being significantly reduced from the value expected for $S = 1/2$ ⁴⁵. The effective magnetic moment expected for $S = 1/2$ is $1.73 \mu_B$, but only $0.68\text{--}0.8 \mu_B$ has been reported for AzBReO_6 ($A = \text{Ba, Sr}$; $B = \text{Mg, Ca, Cd}$) with Re^{6+} ions^{46–49}.

The electronic state of the Re^{6+} ion in CROC is distinct from that of monoanionic 5d magnets. Heteroanionic coordination is advantageous for stabilizing the spin-1/2 state instead of the spin-orbit-entangled J state expected for 5d electrons. As discussed for the optical properties, in CROC, the degeneracy of the 5d orbitals of the Re ion is completely lifted by the CFSs of heteroanionic coordination compounds. First-principles calculations show a 1.4 eV energy separation between the ground state d_{xy} orbital and the first excited state¹⁸ (Fig. 3a). Thus, the orbital angular momentum is quenched. Although the SOI is as large as 0.5 eV in 5d electron systems, the effect of SOI is negligible owing to the large CFSs. The effective magnetic moments obtained from the Curie–Weiss fit to the magnetic susceptibility of CROC at high temperatures range from 1.56 to $1.65 \mu_B$, close to the values expected for spin-1/2 ($1.73 \mu_B$)⁵⁰. In addition, the g -values obtained from electron spin resonance (ESR) experiments are almost isotropic ($1.85\text{--}1.92$) and close to 2 for the spin-only value. Based on these results, the exchange interaction was isotropic, and CROC was studied as a model of an ideal Heisenberg spin quantum magnet with spin-1/2.

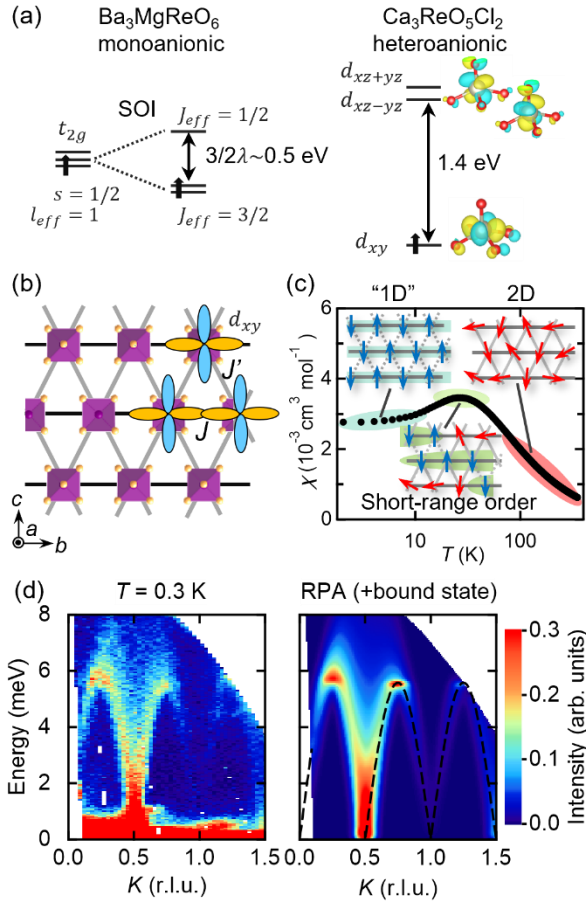


Figure 3. (a) Comparison of electronic states of magnetic ion with $5d^1$ electronic configuration between monoanionic octahedral and heteroanionic square pyramidal coordination. (b) Arrangement of d_{xy} orbitals in CROC forming anisotropic triangular lattice on the bc -plane. (c) Schematic of dimensional reduction in an ATL antiferromagnet shown with the magnetic susceptibility of CROC. The spin alignments of corresponding temperature range are also shown. (d) Inelastic neutron scattering spectra of CROC measured at 0.3 K (left) and simulated by applying random-phase approximation (RPA) to antiferromagnetically coupled spin-1/2 chains (right).

3.2 ANISOTROPIC INTERACTION ORIGINATING FROM ORBITAL STATE

Orbital splitting due to heteroanionic crystal fields affects not only the spin states but also the magnetic interactions between the spins. Because CFs cause electrons to occupy specific orbitals, the magnetic interactions are also anisotropic, reflecting orbital anisotropy.

In CROC, the Re coordination polyhedron does not share ligands with other polyhedra; the distances between the Re ions are 5.5661(1) and 6.3989(3) Å within the bc planes and 5.5515(3) Å with Re ions in different bc planes¹⁹. Considering the Re-Re distances, one would expect the interaction between the bc planes (J'') to be the strongest. However, first-principles calculations estimate that J'' is three orders

of magnitude smaller than the strongest interaction J ($J:J'' = 1:0.0007$)¹⁹. These highly anisotropic interactions are attributed to orbital occupancy, in which electrons occupy the lowest-energy d_{xy} orbitals lying on the bc plane. Therefore, the orbital overlap in the J'' direction was significantly small, and the magnetic interaction was negligible despite the short Re-Re distance. Therefore, CROC can be effectively regarded as a 2D magnet.

In the bc plane, the Re^{6+} ions form a triangular lattice, which is expected to exhibit geometrical frustration. This triangular lattice is not a regular triangular lattice but a triangular lattice stretched in the c -axis direction. In addition, alignment of the d_{xy} orbitals causes highly anisotropic magnetic interactions. Along the b -axis, one pair of electron lobes of the d_{xy} orbital (orange in Fig. 3b) overlaps with those of two neighboring d_{xy} orbitals, which leads to the dominant intra-chain antiferromagnetic exchange, i.e., J . On the other hand, another pair of orbital lobes (blue in Fig. 3b) is arranged in a staggered manner between adjacent chains with a smaller overlap, resulting in the weak interchain exchange of J' . According to first-principles calculations and subsequent high-field ESR experiments, the J'/J anisotropies were estimated to be 0.295¹⁹ and 0.254⁵¹, respectively. It should be noted that direct exchange interactions are sufficiently large even though the transition metals are separated from each other by more than 5 Å.

3.3 MODEL SYSTEM FOR ATL MAGNET

CROC and related materials have recently attracted great attention as model materials for frustrated magnetism on anisotropic triangular lattices (ATL) because of the ideal spin-1/2 state and the two-dimensionality derived from the orbital arrangement^{19,23}.

Theoretically, the spin-1/2 Heisenberg antiferromagnet on an ATL gives rise to intriguing frustration-induced phenomena, called “dimensional reduction”^{52,53}. The ATL is composed of an intrachain interaction J and an interchain interaction J' (Fig. 3b). ATL with $J'/J = 1$ corresponds to a regular triangular lattice, whereas in the limit of $J'/J = 0$ it is identical to a decoupled 1D spin chain. Even with a moderately large interchain interaction ($0 < J'/J \lesssim 0.6$), the competing interactions J' between the chains markedly reduce interchain correlations, and the 2D magnet behaves as an isolated 1D spin chain⁵⁴. As a result, the Tomonaga–Luttinger liquid (TLL) state, which is a characteristic of 1D magnets, is realized at low temperatures.

Many studies have been conducted on Cs_2CuCl_4 , which has a J'/J anisotropy of 0.3. In Cs_2CuCl_4 , a TLL-like state was observed at low temperatures as a continuous excitation of fractionalized spinons carrying spin-1/2 in inelastic neutron scattering experiments^{55,56}. Although the TLL state is expected to be in the ground state, a spiral magnetic order is formed in Cs_2CuCl_4 at a Néel temperature (T_N) = 0.62 K as a result of Dzyaloshinskii–Moriya interactions (DMIs) and interplane interactions. The frustration parameter, J/T_N , which indicates the strength of the suppression of magnetic ordering by frustration, is approximately 7, suggesting a strong influence of interactions other than J and J' . CROC

with similar anisotropy also shows a spiral magnetic order at $T_N = 1.13$ K. However, CROC with high two-dimensionality and ideal spin-1/2 state shows stronger suppression of magnetic order than Cs_2CuCl_4 , with $J/T_N = 35$. In addition, CROC has a large magnetic interaction J , which allows the properties of the ATL to be investigated over a wide temperature range. Therefore, CROC has attracted considerable attention as a better model material for ATL magnets.

The expected dimensional reduction in CROCs has been revealed by the magnetic susceptibility and heat capacity¹⁹: from the Curie–Weiss fit, the Weiss constant was obtained to be 40 K, which indicates that antiferromagnetic interactions are strong enough to induce magnetic ordering below 40 K in the absence of frustration, but no clear magnetic ordering occurred until $T_N = 1.13$ K. In the magnetic susceptibility measurements, a broad peak indicating short-range order was observed at approximately 20 K (Fig. 3c). This temperature dependence of the magnetic susceptibility is not fitted by a 2D model but can be reproduced well by a 1D model. Furthermore, a large Sommerfeld coefficient was observed for the heat capacity at low temperatures, even though CROC is an insulator. The observed large Sommerfeld coefficient corresponding to spinon excitation is a characteristic of 1D magnets. Subsequently, continuous spinon excitation, which is clear evidence of the TLL state, was observed at low temperatures in inelastic neutron scattering⁵⁰ (Fig. 3d) and Raman spectroscopy experiments⁵⁷. Based on these results, the low-temperature state of CROC can be regarded as a 1D magnet.

The interchain interaction J' gives rise to a feature in ATL magnets that distinguishes them from 1D spin chains; because of J' , spinon hopping between neighboring chains is prohibited. Instead, J' causes the formation of a bound spinon pairs (triplons)^{52,53}. These triplons propagate coherently between the chains. In CROC, the interchain hopping of triplons was captured by inelastic neutron scattering experiments as sharply dispersive modes perpendicular to the chain⁵⁰. Magnetic excitation of both spinons and triplons was also observed in the Raman scattering data⁵⁷. The observed temperature dependence of the spinon excitations is different from that expected for 1D spinons and may be a characteristic phenomenon of dimensional reduction. Thus, novel phenomena originating from dimensional reduction, which have not been experimentally verified owing to the lack of model materials, are now being revealed.

3.4 OUTLOOK

Research is currently focusing on CROC, for which single crystals several millimeters in size can be obtained. However, analogous compounds with a $\text{Pb}_3\text{WO}_5\text{Cl}_2$ -type structure should be ideal ATL magnets because of the weaker interplane interactions and prohibited DMIs owing to crystal symmetry. Thus, a spin-liquid state that does not exhibit long-range magnetic ordering, even at the lowest temperatures, may be realized.

Recent high-field ESR measurements revealed that the spiral magnetic order in CROC is stabilized by uniform DMIs⁵¹. Because the incommensurate magnetic order stabilized by

DMIs is expected to host interesting phenomena such as magnetoelectric effects and magnetic skyrmions, the spiral magnetic order in CROC has garnered interest.

As discussed above, the substitution of A and X ions gives rise to anisotropic deformation of the crystal structure (Fig. 1c). Therefore, the magnetic anisotropy J'/J also varies from 0.25 in CROC to 0.45 in $\text{Ba}_3\text{ReO}_5\text{Br}_2$ ²⁰ (Table 1). The change in the magnetic ground state depending on magnetic anisotropy is also of interest.

Orbital degeneracy tends to be reduced in heteroanionic compounds by CFSs with low-symmetry heteroanionic coordination. Thus, the orbital angular momentum is quenched and ideal spin-1/2 quantum magnetism is easily achieved. This is suitable for studying quantum magnetism.

Anisotropic magnetic interactions, which reflect orbital anisotropy, also occurs in many heteroanionic compounds because electrons occupy a specific d orbital. The anisotropy of these interactions may be a source of a new low-dimensional magnetism that is difficult to realize in monoanionic compounds. Therefore, heteroanionic compounds represent a good platform for the development of new low-dimensional magnets.

Heteroanionic coordination often leads to low dimensionality in the crystal structure, and $\text{A}_3\text{MO}_5\text{X}_2$ compounds have layered structures, with oxygen and chlorine forming different layers. A tendency to adopt layered structures was observed in heteroanionic compounds containing oxygen and heavy anions such as Cl, Br, S, and Se. For example, in $\text{Sr}_2\text{CuO}_2\text{Cl}_2$, the parent compound of high- T_c cuprate superconductors, four oxide and two Cl atoms are coordinated to Cu, and Cl selectively occupies the apical oxygen position, forming a layered structure with high two-dimensionality. Owing to its high two-dimensionality, $\text{Sr}_2\text{CuO}_2\text{Cl}_2$ has been studied as a good model material for 2D square lattice quantum magnet^{58,59}. Although heteroanionic compounds have already been recognized as a good platform for quantum magnetism research, and many studies have been devoted to them, future material searches will lead to the discovery of model magnets and associated quantum magnetic phenomena.

4. RELATED MIXED-ANION COMPOUNDS

Several compounds are known in which one halogen and five oxygen atoms coordinate to a metal atom in a square pyramidal configuration, similar to CROC. The most diverse compounds are $\text{A}_2\text{M}^{3+}\text{O}_3\text{X}$, which are analogs of K_2NiF_4 -type layered perovskites, where A = Sr and Ca, M = Sc, V, Mn, Fe, Co, and Ni, and X = F, Cl, and Br^{36,60–67}. See review article for oxyfluorides with related layered perovskite structures⁶⁸. The magnetic properties of the materials were also investigated. In $\text{Sr}_2\text{MO}_3\text{Cl}$ (M = Mn, Co, Ni), a broad peak in the magnetic susceptibility characteristic of low-dimensional magnets has been observed^{36,62,67}, suggesting that the crystal structure and orbital arrangement are responsible for low-dimensional magnetism. In $\text{Sr}_2\text{CoO}_3\text{F}$, spin crossover from high-spin to low-spin states has been reported to occur upon the application of pressure⁶⁹, which is considered a

unique phase transition arising from the change in heteroanionic coordination.

Although the magnetism of A_2MO_3X has been extensively investigated, the optical properties have been neglected. However, it has been reported that Sr_2FeO_3Cl and Sr_2MnO_3Cl exhibit various colors: reddish brown⁶³ and dark green⁷⁰, respectively, possibly because of the intense optical absorption in the visible light region as a result of the square pyramid coordination, which allows $d-d$ transitions. The optical properties of these materials will be investigated in future studies.

There are already several review articles on other heteroanionic compounds such as oxyhalides^{71,72}, oxychalcogenides, oxypnictides⁷³, oxyhydrides⁷⁴, and chalcogenides⁷⁵. Similar to the Pinalite family, many heteroanionic compounds, such as oxyhalides⁷² and oxypnictides⁷³, take a layered structure, while unique crystal chemistry has been revealed in compounds such as chalcogenides⁷⁵ and oxyfluorides⁷¹. Heteroanionic compounds have also been reviewed in terms of their applications: nonlinear optics⁷⁶, semiconductors, photocatalysts, batteries, and superconductors^{72,75,77}. Recent attempts to capture design strategies lead to the on-demand synthesis of designer heteroanionic materials⁷⁸. By incorporating new synthetic ideas, it may be possible to expand the Pinalite family.

5. CONCLUSIONS

In conclusion, the recent progress and future prospects of research on the crystal structures, optical properties, and magnetism of CROC, which was discovered in 2017, and related $A_3MO_5X_2$ compounds have been described. Heteroanionic coordination in heteroanionic compounds strongly affect the d -orbitals of transition metal ions, resulting in unique electronic properties. Since the electronic features of the Pinalite family described in this review (active $d-d$ transitions, complex orbital splitting, and magnetic anisotropy) are universally inherent in many heteroanionic compounds, I hope that this work can stimulate more investigations on optical and magnetic properties of heteroanionic materials. Research on heteroanionic compounds has been active in recent years, and new physical properties and functions have been discovered along the way. Further development is expected in the future.

AUTHOR INFORMATION

Corresponding Authors

*dhirai@nuap.nagoya-u.ac.jp

Funding Sources

This work was partly supported by Japan Society for the Promotion of Science (JSPS) KAKENHI Grants of Numbers JP20H01858, JP22H04462 (Quantum Liquid Crystals), and JP23H04860 and the Toyota Riken Scholar Program from Toyota Physical and Chemical Research Institute.

Notes

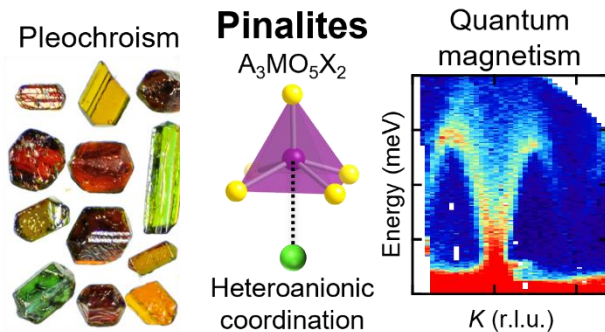
The authors declare no competing financial interest.

REFERENCES

- (1) Kageyama, H.; Hayashi, K.; Maeda, K.; Attfield, J. P.; Hiroi, Z.; Rondinelli, J. M.; Poeppelmeier, K. R. Expanding Frontiers in Materials Chemistry and Physics with Multiple Anions. *Nat. Commun.* **2018**, 9 (1), 772. <https://doi.org/10.1038/s41467-018-02838-4>.
- (2) Kamihara, Y.; Hiramatsu, H.; Hirano, M.; Kawamura, R.; Yanagi, H.; Kamiya, T.; Hosono, H. Iron-Based Layered Superconductor: $LaOFeP$. *J. Am. Chem. Soc.* **2006**, 128 (31), 10012–10013. <https://doi.org/10.1021/ja063355c>.
- (3) Yoichi Kamihara; Takumi Watanabe; Masahiro Hirano, and; Hideo Hosono. Iron-Based Layered Superconductor $La[O_{1-x}F_x]FeAs$ ($x = 0.05-0.12$) with $T_c = 26$ K. *J. Am. Chem. Soc.* **2008**, 130 (11), 3296–3297. <https://doi.org/10.1021/ja800073m>.
- (4) Yamanaka, S.; Hotehama, K.; Kawaji, H. Superconductivity at 25.5 K in Electron-Doped Layered Hafnium Nitride. *Nature* **1998**, 392 (6676), 580–582. <https://doi.org/10.1038/33362>.
- (5) Hiroi, Z.; Kobayashi, N.; Takano, M. Probable Hole-Doped Superconductivity without Apical Oxygens in $(Ca, Na)_2CuO_2Cl_2$. *Nature* **1994**, 371 (6493), 139–141. <https://doi.org/10.1038/371139a0>.
- (6) Kim, Y.-I.; M. Woodward, P.; Z. Baba-Kishi, K.; W. Tai, C. Characterization of the Structural, Optical, and Dielectric Properties of Oxynitride Perovskites AMo_2N ($A = Ba, Sr, Ca; M = Ta, Nb$). *Chem. Mater.* **2004**, 16 (7), 1267–1276. <https://doi.org/10.1021/cm034756j>.
- (7) Imanaka, N.; Okamoto, K.; Adachi, G. Water-Insoluble Lanthanum Oxychloride-Based Solid Electrolytes with Ultra-High Chloride Ion Conductivity. *Angew. Chemie Int. Ed.* **2002**, 41 (20), 3890–3892. [https://doi.org/10.1002/1521-3773\(20021018\)41:20<3890::AID-ANIE3890>3.0.CO;2-M](https://doi.org/10.1002/1521-3773(20021018)41:20<3890::AID-ANIE3890>3.0.CO;2-M).
- (8) Kobayashi, G.; Hinuma, Y.; Matsuo, S.; Watanabe, A.; Iqbal, M.; Hirayama, M.; Yonemura, M.; Kamiyama, T.; Tanaka, I.; Kanno, R. Pure H⁺ Conduction in Oxyhydrides. *Science (80-.)*. **2016**, 351 (6279), 1314–1317. <https://doi.org/10.1126/science.aac9185>.
- (9) Kobayashi, Y.; Tang, Y.; Kageyama, T.; Yamashita, H.; Masuda, N.; Hosokawa, S.; Kageyama, H. Titanium-Based Hydrides as Heterogeneous Catalysts for Ammonia Synthesis. *J. Am. Chem. Soc.* **2017**, 139 (50), 18240–18246. <https://doi.org/10.1021/jacs.7b08891>.
- (10) Hitoki, G.; Takata, T.; Kondo, J. N.; Hara, M.; Kobayashi, H.; Domen, K. An Oxynitride, $TaON$, as an Efficient Water Oxidation Photocatalyst under Visible Light Irradiation ($\lambda \leq 500$ nm). *Chem. Commun.* **2002**, No. 16, 1698–1699.
- (11) Hiramatsu, H.; Yanagi, H.; Kamiya, T.; Ueda, K.; Hirano, M.; Hosono, H. Crystal Structures, Optoelectronic Properties, and Electronic Structures of Layered Oxychalcogenides $MCuOCh$ ($M = Bi, La; Ch = S, Se, Te$): Effects of Electronic Configurations of M^{3+} Ions. *Chem. Mater.* **2007**, 20 (1), 326–334. <https://doi.org/10.1021/cm702303r>.
- (12) Zhao, L.-D.; He, J.; Berardan, D.; Lin, Y.; Li, J.-F.; Nan, C.-W.; Dragoe, N. $BiCuSeO$ Oxyselenides: New Promising Thermoelectric Materials. *Energy Environ. Sci.* **2014**, 7 (9), 2900–2924.
- (13) Shannon, R. D. Revised Effective Ionic Radii and Systematic Studies of Interatomic Distances in Halides and Chalcogenides. *Acta Crystallogr. Sect. A* **1976**, 32 (5), 751–767. <https://doi.org/10.1107/S0567739476001551>.
- (14) Dunn, P. J.; Grice, J. D.; Bideaux, R. A. Pinalite, New Lead Tungsten Chloride Mineral from the Mammoth Mine, Pinal County, Arizona. *Am. Mineral.* **1989**, 74 (7–8), 934–935.
- (15) Grice, J. D.; Dunn, P. J. Crystal-Structure Determination of Pinalite. *Am. Mineral.* **2000**, 85 (5–6), 806–809. <https://doi.org/10.2138/am-2000-5-622>.

- (16) Charkin, D. O.; Lightfoot, P. Synthesis of Novel Lead-Molybdenum and Lead-Tungsten Oxyhalides with the Pinalite Structure, $\text{Pb}_3\text{MoO}_5\text{Cl}_2$ and $\text{Pb}_3\text{WO}_5\text{Br}_2$. *Am. Mineral.* **2006**, *91* (11–12), 1918–1921. <https://doi.org/10.2138/am.2006.2158>.
- (17) Krivovichev, S. ; Armbruster, T.; Depmeier, W. Crystal Structures of $\text{Pb}_5\text{O}_5(\text{AsO}_4)_2$ and $\text{Pb}_5\text{O}_4(\text{CrO}_4)$, and Review of PbO-Related Structural Units in Inorganic Compounds. *J. Solid State Chem.* **2004**, *177* (4–5), 1321–1332. <https://doi.org/10.1016/J.JSSC.2003.11.005>.
- (18) Hirai, D.; Yajima, T.; Nishio-Hamane, D.; Kim, C.; Akiyama, H.; Kawamura, M.; Misawa, T.; Abe, N.; Arima, T.-H.; Hiroi, Z. “visible” 5d Orbital States in a Pleochroic Oxychloride. *J. Am. Chem. Soc.* **2017**, *139* (31), 10784–10789. <https://doi.org/10.1021/jacs.7b05128>.
- (19) Hirai, D.; Nawa, K.; Kawamura, M.; Misawa, T.; Hiroi, Z. One-Dimensionalization by Geometrical Frustration in the Anisotropic Triangular Lattice of the 5d Quantum Antiferromagnet $\text{Ca}_3\text{ReO}_5\text{Cl}_2$. *J. Phys. Soc. Japan* **2019**, *88* (4), 044708. <https://doi.org/10.7566/JPSJ.88.044708>.
- (20) Gen, M.; Hirai, D.; Morita, K.; Kogane, S.; Matsuyama, N.; Yajima, T.; Kawamura, M.; Deguchi, K.; Matsuo, A.; Kindo, K.; Kohama, Y.; Hiroi, Z. Rhenium Oxyhalides: A Showcase for Anisotropic-Triangular-Lattice Quantum Antiferromagnets. *arXiv:2311.06040*. 2023.
- (21) Zikmund, Z. The Crystal Structure of $\text{Ca}_3\text{WO}_5\text{Cl}_2$ and the Configuration of the WO_5^{4-} Ion. *Acta Crystallogr. Sect. B Struct. Crystallogr. Cryst. Chem.* **1974**, *30* (11), 2587–2593. <https://doi.org/10.1107/S0567740874010934>.
- (22) Kitagawa, Y.; Takemura, S.; Hirai, D.; Hiroi, Z.; Ueda, J.; Tanabe, S. Characterization of the Charge Transfer Luminescence of the $[\text{WO}_6]^{6-}$ Octahedron in Ca_3WO_6 and the $[\text{WO}_5]^{4-}$ Square Pyramid in $\text{Ca}_3\text{WO}_5\text{Cl}_2$. *Phys. Chem. Chem. Phys.* **2022**, *24*, 24203–24211. <https://doi.org/10.1039/d2cp02753d>.
- (23) Hirai, D.; Yajima, T.; Nawa, K.; Kawamura, M.; Hiroi, Z. Anisotropic Triangular Lattice Realized in Rhenium Oxychlorides $\text{A}_3\text{ReO}_5\text{Cl}_2$ (A = Sr, Ba). *Inorg. Chem.* **2020**, *59*, 10025–10033. <https://doi.org/10.1021/acs.inorgchem.0c01187>.
- (24) Spitsyn, V.I.; Balashov, V.L.; Kharlanov, A.L.; Lykova, L.N., and Kovba, L. M. Crystal Structure of $\text{Ba}_3\text{WO}_5\text{Cl}_2$. *Sov. Physics, Dokl. (Doklady Akad. Nauk SSSR)* **1985**, *30*, 732–733.
- (25) Symes, R. F.; Cressey, G.; Griddle, A. J.; Stanley, C. J.; Francis, J. G.; Jones, G. C. Parkinsonite, $(\text{Pb}, \text{Mo})_8\text{O}_{18}\text{Cl}_2$, a New Mineral from Merehead Quarry, Somerset. *Mineral. Mag.* **1994**, *58* (390), 59–68. <https://doi.org/10.1180/minmag.1994.058.390.06>.
- (26) Lepore, G. O.; Welch, M. D. The Crystal Structure of Parkinsonite, Nominally $\text{Pb}_7\text{MoO}_9\text{Cl}_2$: A Naturally Occurring Aurivillius Phase. *Mineral. Mag.* **2010**, *74* (2), 269–275. <https://doi.org/10.1180/minmag.2010.074.2.269>.
- (27) Aurivillius, B. On the Crystal-Structure of a Number of Nonstoichiometric Mixed Lead-Oxide Halides Composed of PbO like Blocks and Single Halogen Layers. *Chem. Scr.* **1982**, *19* (3), 97–107.
- (28) Aurivillius, B. Mixed Bismuth Oxides with Layer Lattices I. The Structure Type of $\text{CaNb}_2\text{Bi}_2\text{O}_9$. *Ark. kemi* **1949**, *1* (54), 463–480.
- (29) Aurivillius, B. Mixed Bismuth Oxides with Layer Lattices II. Structure of $\text{Bi}_4\text{Ti}_3\text{O}_{12}$. *Ark. kemi* **1949**, *1*, 499–512.
- (30) Orgel, L. E. Ion Compression and the Colour of Ruby. *Nature* **1957**, *179* (4574), 1348. <https://doi.org/10.1038/1791348a0>.
- (31) Singh, L. The Colour Problem of Ruby. *Nature* **1958**, *181* (4618), 1264–1265. <https://doi.org/10.1038/1811264a0>.
- (32) Gaudry, E.; Kiratisin, A.; Saintavit, P.; Brouder, C.; Mauri, F.; Ramos, A.; Rogalev, A.; Goulon, J. Structural and Electronic Relaxations around Substitutional Cr^{3+} and Fe^{3+} Ions in Corundum. *Phys. Rev. B* **2003**, *67* (9), 94108. <https://doi.org/10.1103/PhysRevB.67.094108>.
- (33) Laporte, O.; Meggers, W. F. Some Rules of Spectral Structure. *J. Opt. Soc. Am.* **1925**, *11*, 459–463.
- (34) E. Smith, A.; Mizoguchi, H.; Delaney, K.; A. Spaldin, N.; W. Sleight, A.; A. Subramanian, M. Mn^{3+} in Trigonal Bipyramidal Coordination: A New Blue Chromophore. *J. Am. Chem. Soc.* **2009**, *131* (47), 17084–17086. <https://doi.org/10.1021/ja9080666>.
- (35) Subramanian, M. A.; Li, J. YInMn Blue - 200 Years in the Making: New Intense Inorganic Pigments Based on Chromophores in Trigonal Bipyramidal Coordination. *Mater. Today Adv.* **2022**, *16*, 100323. <https://doi.org/https://doi.org/10.1016/j.mtadv.2022.100323>.
- (36) Tsujimoto, Y.; Yamaura, K.; Uchikoshi, T. Extended Ni(III) Oxyhalide Perovskite Derivatives: $\text{Sr}_2\text{NiO}_3\text{X}$ (X = F, Cl). *Inorg. Chem.* **2013**, *52* (17), 10211–10216. <https://doi.org/10.1021/ic402008n>.
- (37) Blasse, G.; Brixner, L. H. Luminescence in Gadoliniumchlorotungstate (GdWO_4Cl). *J. Solid State Chem.* **1983**, *47* (3), 368–372. [https://doi.org/https://doi.org/10.1016/0022-4596\(83\)90030-0](https://doi.org/https://doi.org/10.1016/0022-4596(83)90030-0).
- (38) Blasse, G.; Dirksen, G. J.; Brixner, L. H. Luminescence in Trilanthanumtrichlorotungstate ($\text{La}_3\text{WO}_6\text{Cl}_3$). *J. Solid State Chem.* **1983**, *46* (3), 294–305. [https://doi.org/https://doi.org/10.1016/0022-4596\(83\)90153-6](https://doi.org/https://doi.org/10.1016/0022-4596(83)90153-6).
- (39) Ayer, G. B.; Klepov, V. V.; Smith, M. D.; Hu, M.; Yang, Z.; Martin, C. R.; Morrison, G.; zur Loye, H.-C. BaWO_4F_4 : A Mixed Anion X-Ray Scintillator with Excellent Photoluminescence Quantum Efficiency. *Dalt. Trans.* **2020**, *49* (31), 10734–10739. <https://doi.org/10.1039/D0DT02184A>.
- (40) Shi, Y.-F.; Wei, W.-B.; Wu, X.-T.; Lin, H.; Zhu, Q.-L. Recent Progress in Oxyhalogenides as IR Nonlinear Optical Materials. *Dalt. Trans.* **2021**, *50* (12), 4112–4118.
- (41) Wang, J.; Cheng, Y.; Wu, H.; Hu, Z.; Wang, J.; Wu, Y.; Yu, H. $\text{Sr}_3[\text{SnOSe}_3][\text{CO}_3]$: A Heteroanionic Nonlinear Optical Material Containing Planar π -Conjugated $[\text{CO}_3]$ and Heteroleptic $[\text{SnOSe}_3]$ Anionic Groups. *Angew. Chemie Int. Ed.* **2022**, *61* (21), e202201616. <https://doi.org/https://doi.org/10.1002/anie.202201616>.
- (42) Kim, B. J.; Jin, H.; Moon, S. J.; Kim, J.-Y.; Park, B.-G.; Leem, C. S.; Yu, J.; Noh, T. W.; Kim, C.; Oh, S.-J.; Park, J.-H.; Durairaj, V.; Cao, G.; Rotenberg, E. Novel $j_{\text{eff}} = 1/2$ Mott State Induced by Relativistic Spin-Orbit Coupling in Sr_2IrO_4 . *Phys. Rev. Lett.* **2008**, *101* (7), 076402. <https://doi.org/10.1103/PhysRevLett.101.076402>.
- (43) Kim, B. J.; Ohsumi, H.; Komesu, T.; Sakai, S.; Morita, T.; Takagi, H.; Arima, T. Phase-Sensitive Observation of a Spin-Orbital Mott State in Sr_2IrO_4 . *Science* (80-.). **2009**, *323* (5919), 1329–1332. <https://doi.org/10.1126/science.1167106>.
- (44) Takayama, T.; Chaloupka, J.; Smerald, A.; Khalullin, G.; Takagi, H. Spin-Orbit-Entangled Electronic Phases in 4d and 5d Transition-Metal Compounds. *J. Phys. Soc. Japan* **2021**, *90* (6), 062001. <https://doi.org/10.7566/jpsj.90.062001>.
- (45) Abragam, A.; Bleaney, B. *Electron Paramagnetic Resonance of Transition Ions* / A. Abragam and B. Bleaney / 9780199651528 / Oxford University Press Canada; Oxford Classic Texts in the Physical Sciences; Oxford University Press: Oxford, New York, 1970.
- (46) Hirai, D.; Hiroi, Z. Successive Symmetry Breaking in a $j_{\text{eff}} = 3/2$ Quartet in the Spin-Orbit Coupled Insulator $\text{Ba}_2\text{MgReO}_6$. *J. Phys. Soc. Japan* **2019**, *88* (6), 064712. <https://doi.org/10.7566/JPSJ.88.064712>.
- (47) Gao, S.; Hirai, D.; Sagayama, H.; Ohsumi, H.; Hiroi, Z.; Arima, T. Antiferromagnetic Long-Range Order in the 5d¹ Double-Perovskite $\text{Sr}_2\text{MgReO}_6$. *Phys. Rev. B* **2020**, *101* (22), 220412. <https://doi.org/10.1103/PhysRevB.101.220412>.
- (48) Hirai, D.; Hiroi, Z. Possible Quadrupole Order in Tetragonal $\text{Ba}_2\text{CdReO}_6$ and Chemical Trend in the Ground States of 5d¹ Double Perovskites. *J. Phys. Condens. Matter* **2021**, *33*,

- 135603-undefined. <https://doi.org/10.1088/1361-648X/abda79>.
- (49) Ishikawa, H.; Hirai, D.; Ikeda, A.; Gen, M.; Yajima, T.; Matsuo, A.; Matsuda, Y. H.; Hiroi, Z.; Kindo, K. Phase Transition in the $5d^1$ Double Perovskite $\text{Ba}_2\text{CaReO}_6$ Induced by High Magnetic Field. *Phys. Rev. B* **2021**, *104* (17), 174422. <https://doi.org/10.1103/PhysRevB.104.174422>.
- (50) Nawa, K.; Hirai, D.; Kofu, M.; Nakajima, K.; Murasaki, R.; Kogane, S.; Kimata, M.; Nojiri, H.; Hiroi, Z.; Sato, T. J. Bound Spinon Excitations in the Spin-1/2 Anisotropic Triangular Antiferromagnet $\text{Ca}_3\text{ReO}_5\text{Cl}_2$. *Phys. Rev. Res.* **2020**, *2* (4), 043121. <https://doi.org/10.1103/PhysRevResearch.2.043121>.
- (51) Zvyagin, S. A.; Ponomaryov, A. N.; Wosnitsa, J.; Hirai, D.; Hiroi, Z.; Gen, M.; Kohama, Y.; Matsuo, A.; Matsuda, Y. H.; Kindo, K. Dimensional Reduction and Incommensurate Dynamic Correlations in the a $S = 1/2$ Triangular-Lattice Antiferromagnet $\text{Ca}_3\text{ReO}_5\text{Cl}_2$. *Nat. Commun.* **2022**, *13* (1), 6310. <https://doi.org/10.1038/s41467-022-33992-5>.
- (52) Kohno, M.; Starykh, O. A.; Balents, L. Spinons and Triplons in Spatially Anisotropic Frustrated Antiferromagnets. *Nat. Phys.* **2007**, *3* (11), 790–795. <https://doi.org/10.1038/nphys749>.
- (53) Balents, L. Spin Liquids in Frustrated Magnets. *Nature* **2010**, *464* (7286), 199–208. <https://doi.org/10.1038/nature08917>.
- (54) Yunoki, S.; Sorella, S. Two Spin Liquid Phases in the Spatially Anisotropic Triangular Heisenberg Model. *Phys. Rev. B* **2006**, *74* (1), 014408. <https://doi.org/10.1103/PhysRevB.74.014408>.
- (55) Coldea, R.; Tennant, D. A.; Tsvelik, A. M.; Tyliczynski, Z. Experimental Realization of a 2D Fractional Quantum Spin Liquid. *Phys. Rev. Lett.* **2001**, *86* (7), 1335–1338. <https://doi.org/10.1103/PhysRevLett.86.1335>.
- (56) Coldea, R.; Tennant, A.; Tyliczynski, Z. Extended Scattering Continua Characteristic of Spin Fractionalization in the Two-Dimensional Frustrated Quantum Magnet Cs_2CuCl_4 Observed by Neutron Scattering. *Phys. Rev. B* **2003**, *68*, 134424. <https://doi.org/10.1103/PhysRevB.68.134424>.
- (57) Choi, Y.; Lee, S.; Lee, J. H.; Lee, S.; Seong, M. J.; Choi, K. Y. Bosonic Spinons in Anisotropic Triangular Antiferromagnets. *Nat. Commun.* **2021**, *12*, 6453. <https://doi.org/10.1038/s41467-021-26716-8>.
- (58) Greven, M.; Birgeneau, R. J.; Endoh, Y.; Kastner, M. A.; Matsuda, M.; Shirane, G. Neutron Scattering Study of the Two-Dimensional Spin $S = 1/2$ Square-Lattice Heisenberg Antiferromagnet $\text{Sr}_2\text{CuO}_2\text{Cl}_2$. *Zeitschrift für Phys. B Condens. Matter* **1995**, *96* (4), 465–477. <https://doi.org/10.1007/BF01313844>.
- (59) Cuccoli, A.; Roscilde, T.; Vaia, R.; Verrucchi, P. Detection of XY Behavior in Weakly Anisotropic Quantum Antiferromagnets on the Square Lattice. *Phys. Rev. Lett.* **2003**, *90* (16), 167205. <https://doi.org/10.1103/PhysRevLett.90.167205>.
- (60) Yaguchi, H.; Fujii, K.; Tsuchiya, Y.; Ogino, H.; Tsujimoto, Y.; Yashima, M. Ruddlesden–Popper Oxychlorides $\text{Ba}_3\text{Y}_2\text{O}_5\text{Cl}_2$, $\text{Sr}_3\text{Sc}_2\text{O}_5\text{Cl}_2$, and $\text{Sr}_2\text{ScO}_3\text{Cl}$: First Examples of Oxide-Ion-Conducting Oxychlorides. *ACS Appl. Energy Mater.* **2022**, *5* (1), 295–304. <https://doi.org/10.1021/acsaem.1c02828>.
- (61) Sannes, J. A.; Kizhake Malayil, R. K.; Corredor, L. T.; Wolter, A. U. B.; Grafe, H.-J.; Valldor, M. Synthesis and Characterization of Oxide Chloride $\text{Sr}_2\text{VO}_3\text{Cl}$, a Layered $S = 1$ Compound. *ACS Omega* **2023**, *8* (15), 14233–14239. <https://doi.org/10.1021/acsomega.3c01151>.
- (62) S. Knee, C.; A. Zhukov, A.; T. Weller, M. Crystal Structures and Magnetic Properties of the Manganese Oxide Chlorides $\text{Sr}_2\text{MnO}_3\text{Cl}$ and $\text{Sr}_4\text{Mn}_3\text{O}_{8-y}\text{Cl}_2$. *Chem. Mater.* **2002**, *14* (10), 4249–4255. <https://doi.org/10.1021/cm020280c>.
- (63) Ackerman, J. F. The Preparation and Structures of the Alkaline Earth Iron Oxyhalides. *J. Solid State Chem.* **1991**, *92* (2), 496–513. [https://doi.org/https://doi.org/10.1016/0022-4596\(91\)90356-M](https://doi.org/https://doi.org/10.1016/0022-4596(91)90356-M).
- (64) Hector, A. L.; Hutchings, J. A.; Needs, R. L.; Thomas, M. F.; Weller, M. T. Structural and Mössbauer Study of $\text{Sr}_2\text{FeO}_3\text{X}$ ($\text{X} = \text{F}, \text{Cl}, \text{Br}$) and the Magnetic Structure of $\text{Sr}_2\text{FeO}_3\text{F}$. *J. Mater. Chem.* **2001**, *11* (2), 527–532. <https://doi.org/10.1039/b008321f>.
- (65) Kriworuschenko, B.; Kahlenberg, V. On the Symmetry of the $n = 1$ Ruddlesden–Popper Phase $\text{Ca}_2\text{FeO}_3\text{Cl}$. *Cryst. Res. Technol.* **2002**, *37* (9), 958–963. [https://doi.org/10.1002/1521-4079\(200209\)37:9<958::AID-CRAT958>3.0.CO;2-F](https://doi.org/10.1002/1521-4079(200209)37:9<958::AID-CRAT958>3.0.CO;2-F).
- (66) McGlothlin, N.; Ho, D.; Cava, R. J. $\text{Sr}_3\text{Co}_2\text{O}_5\text{Cl}_2$ and $\text{Sr}_2\text{CoO}_3\text{Cl}$: Two Layered Cobalt Oxychlorides. *Mater. Res. Bull.* **2000**, *35* (7), 1035–1043. [https://doi.org/https://doi.org/10.1016/S0025-5408\(00\)00299-3](https://doi.org/https://doi.org/10.1016/S0025-5408(00)00299-3).
- (67) Knee, C. S.; Price, D. J.; Lees, M. R.; Weller, M. T. Two- and Three-Dimensional Magnetic Order in the Layered Cobalt Oxychloride $\text{Sr}_2\text{CoO}_3\text{Cl}$. *Phys. Rev. B* **2003**, *68* (17), 174407. <https://doi.org/10.1103/PhysRevB.68.174407>.
- (68) Tsujimoto, Y.; Yamaura, K.; Takayama-Muromachi, E. Oxyfluoride Chemistry of Layered Perovskite Compounds. *Appl. Sci.* **2012**, *2* (1), 206–219. <https://doi.org/10.3390/app2010206>.
- (69) Tsujimoto, Y.; Nakano, S.; Ishimatsu, N.; Mizumaki, M.; Kawamura, N.; Kawakami, T.; Matsushita, Y.; Yamaura, K. Pressure-Driven Spin Crossover Involving Polyhedral Transformation in Layered Perovskite Cobalt Oxyfluoride. *Sci. Rep.* **2016**, *6* (1), 36253. <https://doi.org/10.1038/srep36253>.
- (70) Knee, C. S.; Weller, M. T. New Layered Manganese Oxide Halides. *Chem. Commun.* **2002**, No. 3, 256–257.
- (71) Leblanc, M.; Maisonneuve, V.; Tressaud, A. Crystal Chemistry and Selected Physical Properties of Inorganic Fluorides and Oxide-Fluorides. *Chem. Rev.* **2015**, *115* (2), 1191–1254. <https://doi.org/10.1021/cr500173c>.
- (72) Di, J.; Xia, J.; Li, H.; Guo, S.; Dai, S. Bismuth Oxyhalide Layered Materials for Energy and Environmental Applications. *Nano Energy* **2017**, *41*, 172–192. <https://doi.org/https://doi.org/10.1016/j.nanoen.2017.09.008>.
- (73) Clarke, S. J.; Adamson, P.; Herkelrath, S. J. C.; Rutt, O. J.; Parker, D. R.; Pitcher, M. J.; Smura, C. F. Structures, Physical Properties, and Chemistry of Layered Oxychalcogenides and Oxypnictides. *Inorg. Chem.* **2008**, *47* (19), 8473–8486. <https://doi.org/10.1021/ic8009964>.
- (74) Kobayashi, Y.; Tsujimoto, Y.; Kageyama, H. Property Engineering in Perovskites via Modification of Anion Chemistry. *Annu. Rev. Mater. Res.* **2018**, *48* (1), 303–326. <https://doi.org/10.1146/annurev-matsci-070317-124415>.
- (75) Ghorpade, U. V.; Suryawanshi, M. P.; Green, M. A.; Wu, T.; Hao, X.; Ryan, K. M. Emerging Chalcogenide Materials for Energy Applications. *Chemical Reviews*. American Chemical Society January 11, 2023, pp 327–378. <https://doi.org/10.1021/acs.chemrev.2c00422>.
- (76) Pan, Y.; Guo, S.-P.; Liu, B.-W.; Xue, H.-G.; Guo, G.-C. Second-Order Nonlinear Optical Crystals with Mixed Anions. *Coord. Chem. Rev.* **2018**, *374*, 464–496. <https://doi.org/https://doi.org/10.1016/j.ccr.2018.07.013>.
- (77) Maeda, K.; Takeiri, F.; Kobayashi, G.; Matsushita, S.; Ogino, H.; Ida, S.; Mori, T.; Uchimoto, Y.; Tanabe, S.; Hasegawa, T.; Imanaka, N.; Kageyama, H. Recent Progress on Mixed-Anion Materials for Energy Applications. *Bull. Chem. Soc. Jpn.* **2022**, *95* (1), 26–37. <https://doi.org/10.1246/bcsj.20210351>.
- (78) Harada, J. K.; Charles, N.; Poeppelmeier, K. R.; Rondinelli, J. M. Heteroanionic Materials by Design: Progress Toward Targeted Properties. *Adv. Mater.* **2019**, *31* (19), 1805295. <https://doi.org/https://doi.org/10.1002/adma.201805295>.



Synopsis

The structure, optical properties, and quantum magnetism of pinalite, a heteroanionic compound with a chemical formula of $A_3MO_5X_2$, are reviewed. The heteroanionic coordination of transition metal ion is the key to the pleochroism and quantum magnetism.



Biography

Daigorou Hirai is an Associate Professor in the Department of Applied Physics at Nagoya University. He received his PhD in materials science from the University of Tokyo (2011). Afterwards, he worked as a postdoctoral fellow in the Department of Chemistry at Princeton University from 2011 to 2013 and in the Department of Physics at the University of Tokyo from 2013 to 2015. Thereafter, he served as a Research Associate at the Institute for Solid State Physics, the University of Tokyo from 2015 to 2022. His research interests include the synthesis, and the structural chemistry of transition-metal based oxides and heteroanionic compounds, in relation to their electronic (magnetic and optical, and superconducting) properties.
